RSC Advances

REVIEW

View Article Online
View Journal | View Issue

Cite this: *RSC Adv.*, 2020, **10**, 27064

Systematic overview of soft materials as a novel frontier for MRI contrast agents

Enrico Gallo,[a] Elisabetta Rosa,[b] Carlo Diaferia,[b] Filomena Rossi,[b] Diego Tesauro[b] and Antonella Accardo *[b]

Received 9th April 2020
Accepted 2nd July 2020

DOI: 10.1039/d0ra03194a

rsc.li/rsc-advances

Magnetic resonance imaging (MRI) is a well-known diagnostic technique used to obtain high quality images in a non-invasive manner. In order to increase the contrast between normal and pathological regions in the human body, positive (T1) or negative (T2) contrast agents (CAs) are commonly intravenously administered. The most efficient class of T1-CAs are based on kinetically stable and thermodynamically inert gadolinium complexes. In the last two decades many novel macro- and supramolecular CAs have been proposed. These approaches have been optimized to increase the performance of the CAs in terms of the relaxivity values and to reduce the administered dose, decreasing the toxicity and giving better safety and pharmacokinetic profiles. The improved performances may also allow further information to be gained on the pathological and physiological state of the human body. The goal of this review is to report a systematic overview of the nanostructurated CAs obtained and developed by manipulating soft materials at the nanometer scale. Specifically, our attention is centered on recent examples of fibers, hydrogels and nanogel formulations, that seem particularly promising for overcoming the problematic issues that have recently pushed the European Medicines Agency (EMA) to withdraw linear CAs from the market.

1. Introduction

Clinical imaging and microscope/fluorescence processing have taken on a valuable role with regards to the methodologies used to produce images of the human body in recent years.[1] These visualization techniques provide benefits and allow a multidimensional evaluation scale, from the imaging of macroscopic anatomical areas and tissues, right down to the microscopic cellular, intra-plasmatic and molecular levels. Consequently, bio-clinical imaging strategies have emerged as some of the most useful devices in healthcare technology for the diagnosis and the treatment of human pathological states (Fig. 1). The evolution of bio-clinical visualizing techniques from radioisotope imaging to more complicated and sensitive methodologies, consisting of computer-assisted tomography (CAT scans), magneto-encephalogram (MEG), positron emission tomography (PET) and ultrasound imaging, has led to innovative improvements in the quality of the healthcare available today.[2] However, every bio-imaging approach available currently suffers from numerous limitations. For instance, the most common limitations of these techniques are the noxious effects of ionizing radiations (X-ray and CAT scan),[3] the damaging impact of radioactivity (in radioscopic techniques),[4] the low sensitivity (*e.g.* magnetic resonance imaging, MRI),[5] the inability to provide resolution smaller than millimeters (as reported for ultrasound imaging)[6] and the general impossibility of differentiating between distinctive pathological compartments (*e.g.* benign and malignant tumors).[7] The urgency of more accurate information about the early cellular and molecular pathological contexts accurately explains the need for extending deep bio-imaging to these organization levels. This understanding may assist the fast detection, screening, diagnosis, and image-guided treatment of life-threatening diseases consisting of cancer, metabolic inborn errors and neurodegenerative diseases. In this direction, nanotechnology could be of great help. Innovative nanomaterials (NMs) and nanostructured platforms (NPs) can help to conquer some of the previously described limitations, combining traditional techniques with modern methods of interest in nanotechnology.[8] In modern science and technology, NMs and NPs have had a revolutionary and radical impact.[9,10] The potential applications of nanoparticles as tracers,[11] markers[12] or contrast agents (CAs)[13] for *in vitro* and *in vivo* optical biological imaging is of remarkable significance. Indeed, nanoparticles can provide several advantages, including tunable physical properties (*e.g.* luminescence and ferromagneticity), a high stability (*e.g.* against photobleaching), the opportunity for targeted delivery, and specific binding through chemical functionalization, multimodality, high sensitivity and selectivity. The aim of this review is to focus

[a]*IRCCS SDN, Via E. Gianturco 113, 80143, Napoli, Italy*
[b]*Department of Pharmacy, Research Centre on Bioactive Peptides (CIRPeB), University of Naples "Federico II", Via Mezzocannone 16, 80134-Naples, Italy. E-mail: antonella.accardo@unina.it*

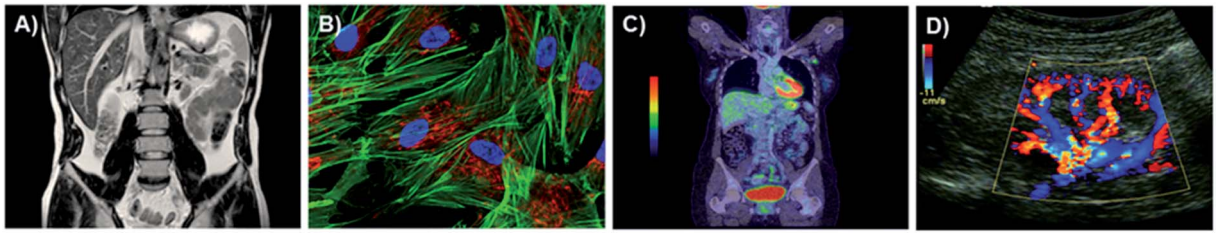

Fig. 1 Techniques: MRI (A), fluorescence (B), PET (C) and SPECT (D).

attention on MRI diagnostic techniques, paying specific attention to the latest soft-based nanomaterials (fibrillary nanostructures, hydrogels and nanogels) proposed as MRI-CAs (see Fig. 2). A description of the advantages of these nanomaterials with respect to the low molecular weight (LMW) ones is also reported. Moreover, in order to give a comprehensive picture of the previously published literature on this specific topic at the end of the review, we report the methodology and the criteria used for the bibliography, explaining all of the consecutive operations related to the identification, screening, eligibility and inclusion steps.

2. Magnetic resonance imaging

Magnetic resonance imaging is a non-invasive medical diagnostic imaging technique presently used to study pathological or other physiological alterations in living tissues, it is used, for example, to reveal and delineate tumor and coronary artery lesions and diseases. MRI signals are generated by the hydrogen nuclei in human tissues. It is worth noting that the human body consists significantly, in part, of water, which is the primary source of the MRI signal in medical imaging applications. MRI signals are generated by measuring parameters associated with the relaxation of hydrogen nuclei. A further magnetic field in the gradient allows retrieval of the spatial information (Fig. 3) in order to obtain 3D MRI-images.[14,15] CAs are widely used to enhance the image resolution in terms of the contrast between normal and abnormal tissues.[16,17] According to the ratio between the two specific parameters, the longitudinal relaxivity (r_1) and transverse relaxivity (r_2), CAs can be classified into two different categories: T1 or T2 CAs. T1 agents generate a positive contrast and are usually based on thermodynamically stable and kinetically inert complexes of paramagnetic ions such as gadolinium.[18] On the other hand, T2 agents generate a negative contrast and are based on paramagnetic compounds such as superparamagnetic iron oxide (SPIO).[19] The parameters of the relaxivity, which represents the efficacy of a contrast agent (CA) at a 1 mM concentration by changing the rate of water proton relaxation, may be used to evaluate the CA performances.[20] The relaxivity of a CA is essentially determined by the molecular reorientation time (τ_R) of the complex and by the exchange lifetime (τ_M) of the water coordinated to the complex. Most of the Gd-complexes used as T1-CAs are based on polydentate chelating agents with a branched or cyclic structure such as diethylenetriaminepentaacetic acid (DTPA) or 1,4,7,10-tetraazacyclododecane-*N*,*N*,*N*,*N*-tetraacetic acid (DOTA). Gd-DTPA (Magnevist®) was the first gadolinium-based MRI-CA; it was authorized for clinical use in 1987. After Magnevist®, a series of other Gd(III) complexes (Gd-DOTA (Dotarem®), Gd-DTPA-BMA (Omniscan®), Gd-HPDO3A (Prohance®), Gd-MS-325

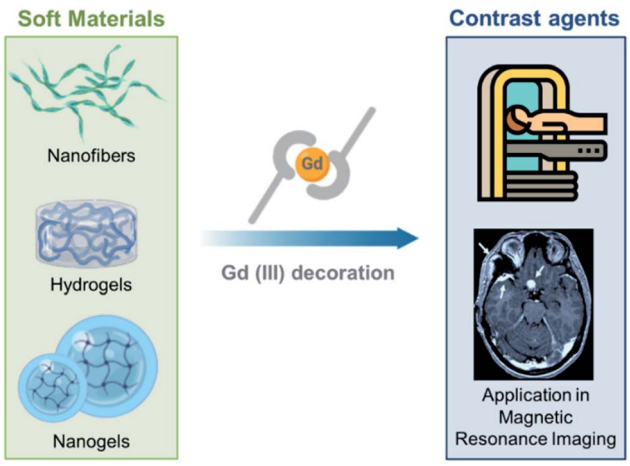

Fig. 2 The class of soft materials includes nanofibers, hydrogels and nanogels. Using appropriate strategies for decoration, these supramolecular aggregates can be functionalized with Gd(III) ions and complexes in order to became suitable for application in MRI as T1-positive contrast agents.

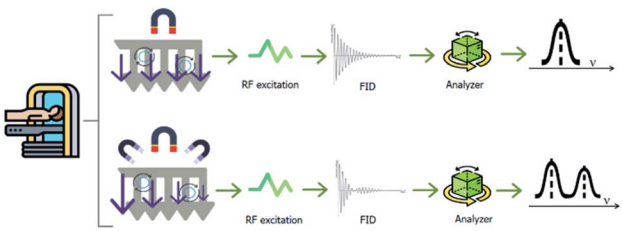

Fig. 3 To obtain an MRI image, the body is located in a uniform magnetic field. Hydrogen nuclei align with the magnetic field and create a net magnetic moment parallel to it. When a radio-frequency pulse (RF excitation) is applied perpendicularly, the net magnetic moment of the nuclei tilts away from the magnetic field. When the RF pulse stops, the nuclei return to the equilibrium initial state (relaxation step). During the relaxation, the nuclei lose energy and a measurable signal, indicated as the free-induction decay (FID), is detected. 3D MRI images can be generated, encoding the FID in each dimension. An additional magnetic field in the gradient changes the FID as a function of the proton 3D position.

(Ablavar®), Gd-DTPA-BMEA (OptiMARK®), EOBDTPA31 (Eovist®) and Gd-BOPTA (Multihance®)) were approved for diagnostic applications. These T1-agents with an LMW have a range of relaxivities between 4 and 5 mM^{-1} s^{-1} at 20 MHz and 310 K. Owing to their LMW, classical Gd-complexes rapidly extravasate after their intravascular administration. This extravasation causes a reduction in the contrast from the neighboring tissues. In contrast, the extravasation phenomenon can be extensively limited using multimeric gadolinium complexes or macromolecular/supramolecular CAs with a molecular weight of more than 30 kDa. Several strategies have been proposed to obtain macromolecular CAs. One of them utilizes the insertion of a hydrophobic substituent capable of binding with high affinity serum proteins such as human serum albumin (*e.g.* Ablavar® and MP-2269)[21] on the Gd-complex. Alternatively, the synthesis of polymeric scaffolds decorated with multiple copies of the CA have been suggested.[22–25] Another approach, explored over recent years, is the non-covalent association between the protein avidin and the Gd-complex–biotin adduct that brings about the formation of a macromolecular system containing four Gd-complexes.[26] An analogous non-covalent approach is the interaction between cyclodextrin and its host ligand.[27] Alternatively, gadofullerenes and gadonanotubes have been proposed as a new generation of high performance CAs for MRI.[28–30] These carbon nanostructures were found to be 20-times more effective than the current clinical CAs with a relaxivity value up to 180 mM^{-1} s^{-1} per gadolinium ion. Beyond the high relaxivity value, these nanosystems exhibit a low *in vivo* dissociation of the metal ion, a decrease in the uptake by the reticulo endothelial system (RES) and an increase in the clearance.[31] All of these macromolecular compounds exhibit an increase in their relaxivity according to the unit dose of the paramagnetic ion. This increase is caused by the coexisting presence of a high number of gadolinium complexes for each molecule and the longer τ_R value with respect to the LMW-CAs, such as Magnevist® or Dotarem®.

More recently, and with the same purpose, supramolecular aggregates, such as micelles and liposomes, have also drawn significant attention as diagnostic agents in nanomedicine.[32] The pharmacological properties of these systems, including the relaxivity, biodistribution and clearance can be simply settled and controlled by modifying their physicochemical properties such as the size, surface charge or membrane composition.[32] These multi-gadolinium CAs can be formulated in agreement with two different procedures: (i) Gd-complexes can be entrapped within the internal compartments of these nanostructures; or (ii) they can be covalently linked to a hydrophobic chain able to self-assemble.[32] In the first method, minimal exchange of the bulk water with the CA could result and the relaxivity of the entrapped paramagnetic species could be noticeable low as a consequence of the low permeability of some lipidic membranes. In the second method, it is important to distinguish between liposomal and micellar aggregates. The micellar structures present in the gadolinium complexes are entirely exposed on the external surface of the aggregate. Otherwise, in liposomes the metal complexes are distributed between their inner and the outer compartments. The assignment of Gd-complexes between the two liposomal layers could be different, and each contribution has to be considered.[33] In this instance, the complexes in the inner layer provide a contribution to the paramagnetic relaxation rate for liposomal structures only with a highly permeable membrane, in which the water exchange rate is very fast. Macro- and supramolecular CAs exhibit a typical NMRD (nuclear magnetic relaxation dispersion) profile with a peak at high frequencies (clinically relevant field strengths). This characteristic peak is caused by the increase in the rotational correlation times. Furthermore, to analyze the data for the longitudinal ^{17}O and ^{1}H relaxation rates, the Solomon–Bloembergen–Morgan model, adapted in agreement with the Lipari–Szabo approach, must be used.[34,35]

This approach differentiates between two statistically independent motions: a rapid local motion of the Gd(III) complex governed by means of a correlation time (τ_l) and a slower global motion of the entire supramolecular construct governed by a correlation time (τ_g). The degree of local to global influence related to the overall motion is established by another model-free parameter (S^2) that can assume a value ranging between 0 and 1. Both τ_l and τ_g can be affected by several structural features of the amphiphilic gadolinium complex, such as the length and the hydrophobicity of the side chain.

3. Gd-CAs based on fibers

Organic and inorganic fibrillary nanostructures have been recently proposed as platforms for biomedical applications.[36,37] Owing to their excellent mechanical strength, high porosity and easy fabrication, fibers could be employed as potential delivery systems of active pharmaceutical ingredients (APIs) such as therapeutic and/or diagnostic agents, for the fabrication of wound dressings and regenerative medicine. In this scenario,

Table 1 Gadolinium complex, relaxivity value at a 1 mM concentration and references for fibrillary nanostructures

System	Gd(III) complex	r_{1p} (mM^{-1} s^{-1})	Ref.
PA 5	Gd-DO3A	16.6 (pH = 4), 13.2 (pH = 10)	40
DOTAMA-PEG_6-F4, DTPAMA-PEG_6-F4	Gd-DOTA, Gd-DTPA	14.0, 14.8	41
FF-DOTAMA-FF	Gd-DOTA	11.5	44
$2NaI_2$	Gd-DOTA	12.3	45
Cha-DOTA/C-Cha (2 : 8 mol mol^{-1}), (8 : 2 mol mol^{-1})	Gd-DOTA	19.5, 17.2	48
PpiX-PEG8-SSSPLGLAK-Ppdf	Gd-DOTA	28.2 (sphere), 51.5 (fiber)	49
SMNs/FMNs	Gd-DOTA	15.6 (sphere), 18.5 (fiber)	51

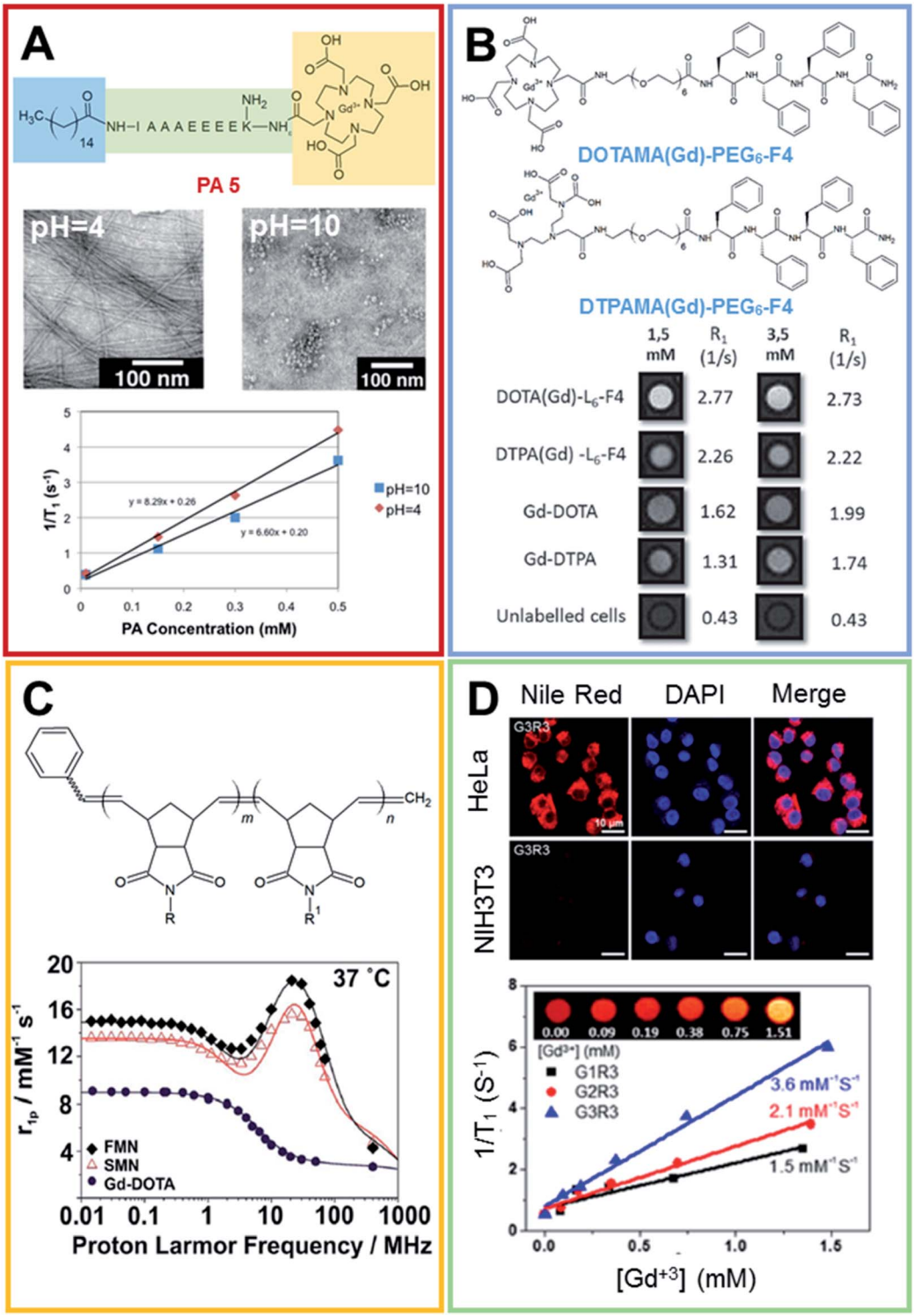

Fig. 4 (A) Chemical formula for the PA 5 compound, the peptide sequence of PA 5 is reported according to the one code letter. TEM images (0.5 mM solution of PA 5) at pH 4.0 (on the left) and 10.0 (on the right). T1 relaxivity graph of PA 5 under basic and acidic conditions (adapted with permission[40] 2012-American Chemical Society). (B) Chemical structure of DOTAMA(Gd)-PEG_6-F4 and DTPAMA(Gd)-PEG_6-F4. T1-weighted MR-images of pellets of the J774A.1 cell line labelled with 1.5 and 3.5 $\times 10^{-3}$ mol L^{-1} of the two Gd-complexes. The relative observed relaxation rates are reported too (reproduced with permission from ref. 41). (C) Chemical structure of Gd^{3+}-containing an amphiphilic block copolymer. R and R′ can be a phenyl group or a modified Gd-DOTA complex (norbornenyl-Gd-DOTA monoamide). ^{1}H NMRD profiles for Gd-DOTA, spherical and fibrillar micellar nanoparticles (reproduced with permission,[51] published by The Royal Society of Chemistry). (D) Laser scanning microscopy images of HeLa and NIH3T3 cells lines treated with Nile red-loaded porous networks of Gd^{3+}-G3R3 (1 h after incubation): left, Nile red (red); middle, nuclei stained with DAPI (blue); and right, merged images. T1 relaxivity plots of Gd^{3+}-chelating nanostructures (0.2 mM) as a function of the Gd^{3+} concentration ([Gd^{3+}]) (4.7 T, 25 °C) and (inset) T1-weighted MR images of Gd^{3+}-G3R3 (adapted with permission,[50] copyright 2017-American Chemical Society).

there are various previously published examples of MRI-CAs based on fibrillary nanostructures (see Table 1). Most of these were obtained for the self-assembly of peptide sequences. Peptides are versatile molecules, which present various advantages such as biocompatibility, a low-cost and synthetic variability. Owing to their appealing features, they have been proposed as antimicrobial/antiviral agents, therapeutic/diagnostic agents, or molecules for achieving passive or active targeting on cells. Moreover, in the last two decades researchers have begun to use peptides as useful functional molecules for obtaining novel biocompatible supramolecular architectures including nanotubes, nanofibers, nanospheres, nanovesicles and hydrogels.[38]

These supramolecular nanostructures can be obtained by self-assembly of several types of peptides, including cyclic and linear peptides, amphiphilic peptides (PAs), and α-helical and β-sheet peptides.[39] In this context, amphiphilic peptides and aromatic peptides were found to self-assemble into well-ordered nanofibers. In 2012 Goldberger *et al.*[40] synthesized a series of self-assembling PA molecules as pH sensitive reversible systems for *in vivo* imaging and drug delivery applications. These PAs, containing a hydrophobic alkyl tail, a β-sheet-forming peptide sequence and a charged amino acid sequence, were found to give a transition from single molecules or spherical micelles into self-assembling nanofibers upon acidification (from pH 7.4 to 6.6). Structural studies showed a fast and reversible transition from the random coil, which corresponds to isolated molecules in solution, to a β-sheet structure that supports the existence of fibers, at a pH of 6.6. By varying the β-sheet propensity of the amino acids in the β-sheet-forming region, the transition pH can be finely modulated. Moreover, it was observed that after the modification of the peptide sequence at the C-terminus with the gadolinium complex [1,4,7-tris(carboxymethylaza)cyclododecane-10-azaacetylamide (Gd-DO3A)] the structural transition occurs at a more acidic pH value (5.7–6.0). This result could probably be ascribed to the steric hindrance and the additional hydrophilicity of DO3A. Relaxivity studies using a 1.5 T magnet showed values of 8.3 and 6.6 mM^{-1} s^{-1} for 500 μM of the product at pH 4 and 10 respectively (Fig. 4A). Recently, Diaferia *et al.*[41,42] developed several examples of aromatic peptide conjugates for use as MRI-CAs. The idea of using aromatic short peptides (containing two or three residues) as building blocks to prompt fiber formation originated from the large amount of published literature on the ultra-short homodipeptide Phe–Phe (FF or F2), a dipeptide identified for the first time by Gazit in 2003 as an aggregating core motif for the Aβ-amyloid peptides (Aβ1-40 and Aβ1-42).[43] This peptide self-organizes efficiently into well-ordered tubular architectures, but according to the experimental conditions (pH, temperature, solvents and preparation methods) it can assemble into nanostructures with a different morphology. Initially, the authors prepared conjugates in which the Gd-complexes (Gd-DTPA or Gd-DOTA) were bound on diphenylalanine (F2) or tetraphenylalanine (F4) using a PEG spacer.[41] Only tetraphenylalanine derivatives, DOTAMA(Gd)-PEG_6-F4 and DTPAMA(Gd)-PEG_6-F4, exhibited the capability to form fibrillary nanoaggregates, in which the peptides were arranged in a β-sheet conformation with an antiparallel alignment along the fiber axis. Relaxivity studies indicated that both the DOTA and the DTPA conjugates exhibited a r_{1p} (~15 mM^{-1} s^{-1} at 20 MHz) three-fold higher than the classical LMW CAs. Analysis of the relaxometric parameters, with particular reference to the τ_R, suggested that the PEG spacer significantly increases the internal motility of the Gd-complexes with respect to the overall fibril-like structures. *In vitro* assays demonstrated the ability of both the nanostructures to enhance the MRI cellular response on the J774A.1 mouse macrophage cell line (Fig. 4B) and their high biocompatibility in the 0.5–5.0 mg mL^{-1} concentration range. In order to improve the relaxivity of these nanostructures, the same authors synthesized novel conjugate analogues in which the position of the Gd-complex in the aromatic sequence[44] and the aromaticity/hydrophobicity of the peptide framework were changed.[45] In the first study they investigated how the change in the position of the Gd-complex from the N-terminus to the center of the F4-motif could affect both the structural and relaxivity properties of the aggregates. The results highlighted that when the Gd-complex is located at the center of the aromatic peptide sequence (FF-DOTAMA(Gd)-FF), there is a reduced tendency to self-assemble and the fibrillary networks only appear above a concentration of 50 mg mL^{-1}. This reduced tendency to self-organize also causes a decrease in the observed relaxivity value (11.5 mM^{-1} s^{-1}).[44] In the second study, the role of the aromaticity on the structural organization and on the relaxometric behavior was studied by replacing the F residue with the non-coded amino acid naphthylalanine (2-Nal).

As expected, the increase in the aromaticity corresponds to a major tendency to self-assemble (critical aggregation concentration ~ 0.1 mg mL^{-1}) and stable amyloid like nanostructures can be observed for Gd-$2Nal_2$ for a concentration of around 1.0 mg mL^{-1}. A further increase in the concentration (above 20 mg mL^{-1}) brought about the formation of a hydrogel such as those of other PEGylated analogues.[46,47] In line with the other systems previously described, these gels exhibited a r_{1p} value of 12.3 mM^{-1} s^{-1} at 20 MHz and a satisfactory capability to encapsulate anticancer drugs, such as doxorubicin. According to this strategy, in 2016 Lee and coworkers proposed a similar multifunctional theranostic nanoplatform, loaded with Gd-complexes and doxorubicin, for application in personalized medicine.[48] These targeted fibrillary nanostructures were obtained by mixing two different peptide monomers: the first one composed of an aggregative motif and the homing peptide octreotide (OCT) and the second one composed of the same aggregative motif and the Gd-DOTA complex. The common motif contains four hydrophobic amino acids (*e.g.* Phe, or cyclo-hexylalanine, Cha) alternating with four lysine residues and a PEG linker with four ethoxylic units. The relaxivity values of the different nanofibers, prepared at several molar ratios, fall in the 17.1–19.5 mM^{-1} s^{-1} range. As expected, the slight differences in the r_1 values are strictly related to the dimensions of the resulting nanostructures. *In vitro* assays carried out on MCF-7 cancer cells overexpressing the SST receptor (SSTR) indicated the capability of targeted theranostic fibrils to selectively deliver doxorubicin, with a very

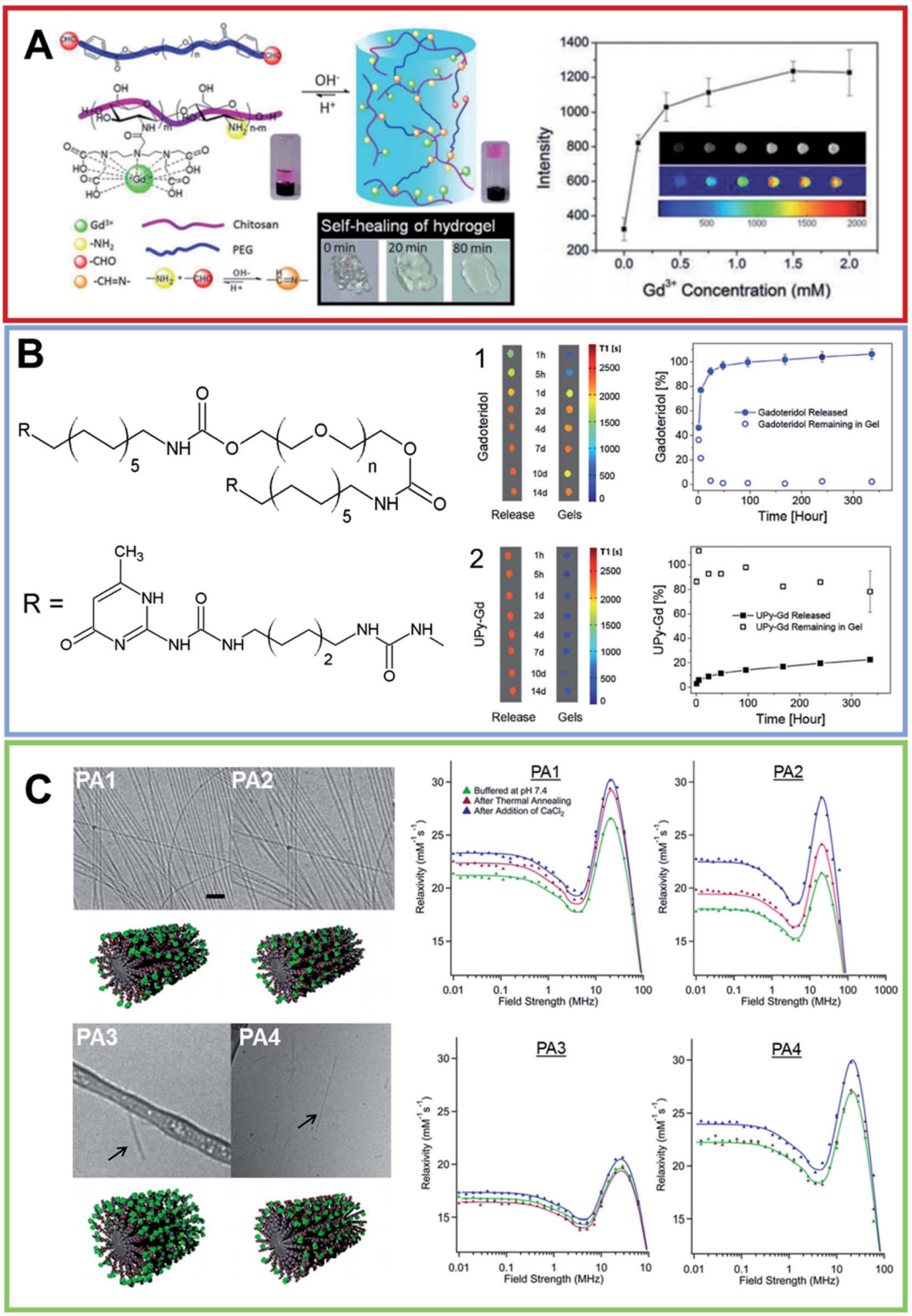

Fig. 5 (A) On the left, schematic illustration of the formation of pH-sensitive injectable hydrogel composed by a modified PEG polymer (blue ribbon) and a DTPA-decorated chitosan (purple ribbon). The hydrogel self-healing feature is reported too. On the right, MRI intensity of the visible hydrogel as a function of the Gd(III) concentration (from ref. 57. Reproduced by permission of The Royal Society of Chemistry). (B) Chemical structure for the bifunctional hydrogelator containing ureidopyrimidinone (UPy). 10 wt% UP-PEG hydrogels T1-weighted 1.5 T MRI scans reported in pseudo-color of the released solution and for the gels. Hydrogels contain either (1) 1×10^{-3} mol L^{-1} Gadoteridol or (2) 1×10^{-3} mol L^{-1} UPy-Gd(III) modified monomers. The relative release curves are reported too (arranged with permission[59]). (C) On the left, Cryo-TEM of PAs conjugates in 10 mmol L^{-1} in Tris buffer after a process of thermal annealing (80 °C for 30 min) and their relative molecular graphical representation. The scale bar represents 200 nm and Gd macrocycles are represented as green elements. On the left, the NMRD profiles for all PAs at three different conditions recorded at 37 °C and a PAs concentration of 2 mmol L^{-1} (adapted with permission,[67] copyright 2014-American Chemical Society).

low toxicity during 24 h of incubation. Another example of a smart theranostic agent based on fibrillary nanostructures was recently proposed by Han *et al.*[49] In this case, the nanostructure was obtained thanks to the self-assembly of PpiX-PEG8-SSSPLGLAK (DOTAMA)-PEG_6-F4 (named as Ppdf-Gd), a monomer containing four different moieties: (i) the polymer-peptide PEG_6-F4 previously described; (ii) a matrix metalloproteinase-2 (MMP-2) responsive chimeric peptide (PLGLA); (iii) the Gd-DOTA complex; and (iv) the photosensitizer protoporphyrin IX (PpiX). Under physiological conditions, the monomer aggregates into spherical nanoparticles having a r_{1p} value of 28.17 mM^{-1} s^{-1}. *In vivo*, the overexpressed MMP-2 hydrolyzes the cleavable peptide sequence, releasing the PEGylated-PpiX fragment, as well as LAK-DOTAMA(Gd)-PEG_6-F4 in the tumor site. Owing to the aromatic stacking interaction among the Phe residues and the hydrogen bond within the peptide chain, this latter fragment self-assembles in long fibers. This sphere-to-fiber transition enhances both the *in vivo* tumor accumulation and the relaxation rate of the Gd-complex (r_{1p} = 51.52 mM^{-1} s^{-1}). The therapeutic efficacy of Ppdf-Gd was assessed in SCC-7 tumor bearing nude mice. The results showed that tumors in the Ppdf-Gd group that underwent light irradiation were significant smaller than other groups. Furthermore, the serum analysis carried out on the blood of mice indicated that the Ppdf-Gd, with and/or without light irradiation, did not cause any toxicity in the liver, kidneys and heart.

In 2017 Lee *et al.* developed supramolecular theranostic nanoagents with antimicrobial activities.[50] These agents, based on the self-assembly of amphiphatic antimicrobial peptides (AMPs), are capable of Gd^{3+} conjugation and tumor-targeting in aqueous solution. In detail, a series of AMPs (G1, G2, G3) consisting of *N*-alkyl/aryl pyrazole (Py) amino acids and arginine (Arg) building blocks were designed. Py and Arg were responsible for upholding the hydrophobicity and positive charge of the peptides. Then, the building block structure was covalently decorated with the addition of tripeptide glycine–histidine–lysine (GHK), for the Gd^{3+} coordination, or linked to cyclic arginine–glycine–aspartic acid (cRGD) (R1, R3), for the recognition of αvβ3 and αvβ5 integrin receptors expressed on tumor cells. Several Gd-complexed co-assembled AMPs (Co-AMPs, G1R1, G2R1, G3R1, G1R3, G2R3, G3R3) were prepared by mixing GHK-AMP and cRGD-AMP peptides of various lengths in deionized water, these peptides were obtained by repeating Py or Arg building units. Co-AMPs were successfully tested as carriers, encapsulating the drug doxorubicin. *In vitro* studies showed a relatively low cytotoxicity in HeLa cells (human tumor cell line), antimicrobial activities against *E. coli* and *S. aureus* and biocompatibility in theranostic treatments (Fig. 4D). Moreover, the r_1 value of Gd^{3+}-G3R3 Co-AMPs (3.6 mM^{-1} s^{-1}) showed the strongest magnetic resonance (MR) signal (Fig. 4D).

Beyond the fibrillary CAs obtained from the self-assembly of PAs and aromatic peptides, there is also an example of supramolecular CAs prepared by direct polymerization of amphiphilic block copolymers, in which the hydrophilic block consists of a modified Gd-DOTA moiety (Fig. 4C).[51] The resulting nanostructures were proposed as promising candidates for the treatment and diagnosis of peritoneal malignancies. The copolymers assemble, leading to two different phases of micellar nanoparticles (MNs): one entirely spherical (SMN) and the other predominantly fibrillar (FMN). The NMRD profiles show enhanced relaxivity over Gd-DOTA (15.6 mM^{-1} s^{-1} and 18.5 mM^{-1} s^{-1} for SMN and FMN respectively), with the same order of magnitude of other nanoparticles and polymer-based systems. *In vivo* preliminary studies, following intraperitoneal injection in mice, indicate that the nanoparticle formulations are retained *in situ* for longer than Gd-DOTA, undergoing less clearance through renal excretion. These data were also confirmed by *ex vivo* analyses.

4. Hydrogels

Hydrogels represent the first class of biomaterials planned for use in the human body, and they have found widespread biomedical applications. Hydrogels are viewed as a three-dimensional network of natural and/or synthetic polymers, having the ability to absorb a large amount of water molecules or biological fluids. The most common constituents include polyvinyl alcohol (PVA), sodium polyacrylate, acrylate polymers and generally copolymers with an abundance of hydrophilic groups. Recently, innovative methods for hydrogel synthesis have extended the field of biomaterials, to concern the unusual aspects of the synthesis of hydrogels, the rewards and limitations, together with particular aspects of synthetic hydrogels such as the composite, biodegradable, superabsorbent and stimuli-sensitive ones.[52,53] They have found application in surgical procedures, as scaffolds for tissue engineering[54] or as the basis for the administration of therapeutic and/or diagnostic agents.[55] Surgical therapies or tissue regenerations can be monitored in real-time, exploiting non-invasive techniques. MRI, indubitably, fulfills these requirements. Despite this interest, few examples of *in vivo* imaging hydrogels based on Gd^{3+}, especially injectable hydrogels, have been reported.

Seliktara *et al.* prepared fluorescence/MRI probes based on two novel hydrogels, in order to identify the host angiogenic response to implants.[56] The Gd-DTPA complex was covalently conjugated to VEGF-bearing biodegradable PEG–fibrinogen hydrogel implants, and they were used to document the *in vivo* degradation and release of bioactive constituents in a stem cell rat implantation model. Hydrogels based on carbohydrates derivatives exhibit many desirable advantages, such as biocompatibility and an easily available feedstock. Moreover, they are pH sensitive, can be injected and are self-healing. These properties allowed the preparation, at room temperature, of hydrogels based on chitosan (CH) and PEG. Zhuo *et al.*, obtained them by mixing, in aqueous solutions, CH functionalized with DTPA and the PEG end-capped with aryl-aldehyde[57] (Fig. 5A). The obtained macromolecular Gd-complex in solution is able to tolerate steam sterilization, and it retains the paramagnetic MRI enhancement contrast effect. The value of the relaxivity is not affected by the covalent bond, showing almost the same value when the complex electrostatically interacts with CH. However, the covalent bond does not allow complex diffusion and the hydrogel can hold back Gd^{3+} ions for 35 d,

according to the *in vivo* tests. Therefore, the gradual loss of intensity is only a result of the hydrogel degradation from the surface to the core of the structure. Consequentially, the shape and global state of the hydrogel can be visualized by a non-invasive MRI, offering a scaffold to monitor long-term reporting of implants. Hydrogels based on enzymatic sensitive carbohydrates were also reported by Hilborn *et al.*[58] They achieved injectable gadolinium-labeled HA, dually functionalized with Gd-DTPA and chemoselective groups. The *in situ* crosslinking of hyaluronic acid (HA) was based on the hydrazone bond. *In vitro* T1-weighted MR images of Gd-labeled hydrogels decreased in function at different time points of degradation. *Ex vivo* MRI confirmed that the resulting hydrogels show noteworthy differences in contrast with the surrounding tissues. At the same time Dankers *et al.*, embedded an ureidopyrimidine modified Gd-DOTA (UPy Gd) complex (Fig. 5B) in an injectable supramolecular ureidopyrimidinone based hydrogel (UPy-PEG).[59] This hydrogel prevents the complex UPy Gd from diffusing, giving a high contrast and precise information on the 3D shape and location, better than Gadoteridol (Prohance®) loaded in UPy-PEG. The UPy-Gd labeled hydrogel is perfectly visible *in vivo* after minimally invasive catheter injection in a beating heart. Despite these results, this supramolecular system has not reached a clinical standard yet. In addition, Parigi *et al.* investigated the Prohance® relaxometric enhancement in HA hydrogels used as a tissue model.[60] This effect can be attributed to a reduced diffusion coefficient in the outer sphere water molecules or by the additional contribution of fast exchanging second-sphere water molecules, with a residence time longer than several hundred nanoseconds. Another class of hydrogels can form self-assembling peptide amphiphiles (PAs). PAs are molecules in which a hydrophilic peptide is covalently bound on a hydrophobic moiety (one or more alkyl chains). The chemical nature of PAs prompts them to self-aggregate in water in highly ordered nanostructures, such as one-dimensional cylindrical micelles.[61] The very close packing of peptide moieties on the nanostructure surface causes their β-sheet arrangement during the self-assembly process. The high biocompatibility and biodegradability of the PAs-based materials suggests their potential employment in nanomedicine as 3D-scaffolds for tissue engineering[62] or as delivery systems for CAs and/or anticancer drugs.[63] In the latter role, the peptide sequence could play both a structural and biological role in the recognition mechanism.[64] One of the first examples of self-assembled MRI-CAs based on PA nanofibers was reported by Stupp and coworkers in 2005, for the *in vivo* detection (migration and degradation) of PA biomaterial based scaffolds.[65] The authors synthesized two branched PAs, both of them containing the palmitic acid as hydrophobic portion, the cyclic DOTA as chelating agent and a peptide sequence as β-sheet inducer (V3A3). Moreover, the two PAs (PACA1 and PACA2) differ for the presence of an additional sequence on V3A3, that is RGDS in PACA1 and C4 in PACA2. The repetition of four cysteins was introduced to achieve the reversible crosslinking of the supramolecular aggregate. Under physiological conditions, Gd-PACA1 forms well-ordered fibers longer than 100 nm and with a width of around 20 nm; whereas uncrosslinked Gd-PACA2 generates spherical micelles (10 nm). Both the nanostructures exhibited relaxivity values higher than the corresponding LMW Gd-complexes (14.7 mM^{-1} s^{-1} for self-assembled Gd-PACA1, 22.8 mM^{-1} s^{-1} for uncrosslinked Gd-PACA2 and 20.8 mM^{-1} s^{-1} for crosslinked Gd-PACA2, respectively). The different r_{1p} observed for the two PAs could be attributed to the different flexibility of the Gd-complex into the supramolecular nanostructure. Indeed, it was observed that the change of position of the chelating agent (close to the alkyl chain) causes a significant increase in the measured relaxivity (21.5 mM^{-1} s^{-1}). In their next study, the same authors used these self-assembled PACA1 nanofibers to dope a PA gel at 1% wt. The PA sequences chosen for the hydrogel preparation were two epitopes typically used for neuronal stem cell differentiation (IKVAV and YIGSR). The resulting hydrogels were non-invasively imaged.[66] The encouraging results prompted the authors to develop four novel DOTAMA(Gd)-PACAs to follow the *in vivo* fate of implanted PA gels in the tibialis anterior muscle of mouse limbs over several days.[67] As for the previously described PAs, all of the PAs contain the V3A3 motif to induce the formation of β-sheet structures plus three glutamic acid residues (E3), that allow an increase of the water solubility and the coordination of divalent cations during the crosslinking with Ca(II) ions. These PAs crosslinked hydrogels, which exhibit a relaxivity value higher than 20 mM^{-1} s^{-1} at 60 MHz, were tested *in vivo* in a mouse model. The results indicated the persistence of the PA gel in the legs over a 4 d period (Fig. 5C).

The other goal pursued by researchers is the delivery of therapeutic and/or diagnostic agents to the desired tissues.[68] From this perspective, several MRI contrast agents containing hydrogels have been formulated in recent years. For example, Cheng *et al.*[69] investigated the theranostic ability of a PEG hydrogel used as a carrier. The effect of Apatinib containing Gd-PEG was studied by injecting this supramolecular structure into a hepatocellular carcinoma model of HepG2 in nude mice. MRI and histomorphology showed that the necrotic area in carcinoma was larger in the Apatinib-Gd-PEG hydrogel treated mouse group, compared with three groups treated with Apatinib, the Gd-PEG hydrogel and saline solution. Moreover, after the treatment, the angiogenesis (VEGF receptor 2) of HepG2 appears to be reduced with respect to the others three groups. Another material with theranostic applications was reported by Yan *et al.*[70] This material, represented by a metallo-folate hydrogel as printable biomaterials, was obtained step by step and has strong mechanical properties. The pterin rings, through hydrogen bonding, form tetramers that evolve into nanofibers by π–π stacking. The zinc ion allows larger-scale fibrils to be achieved that form networks with further crosslinked fibrils. This hydrogel material is able to be doped by Gd^{3+} increasing the value of 1/T1 in the function of the ion concentration. *In vivo* MRI experiments clearly revealed tumor HeLa cells in nude mice.

As an alternative, the PEG network can be crosslinked with bioactive peptides to obtain hydrogels. In this context, Stevens *et al.* developed a multimodal platform system for potential theranostic use in tissue engineering and drug delivery applications.[71] The central moiety of the peptide contains the

heparin binding region amino acid sequence (LRKKLGKA), whereas both the C- and the N-terminus contain a cysteine residue, which assists the hydrogel crosslinking achieved by a Michael addition between the thiol groups of Cys and 4-arm PEG-acrylate. The heparin-binding peptides were further functionalized on the lysine residues with Gd-DOTA. The resulting hydrogel, loaded with cardiac stem cells (CSC), displays mechanical properties resembling cardiac tissue and maintains cell metabolic activity. This platform system improves luciferase-expressing-CSC (CSC-Luc2) retention in the myocardia of mice and shows promising properties for use in further applications enhancing existing cell therapies. In order to improve the MR performance, Chen *et al.* opted to use the Gd(III) ion to generate the formation of supramolecular nanofibers and hydrogels.[72] In this case, hydrogelations were achieved by adding the Gd^{3+} ion to the nanofiber dispersion of the sequence naphthalene-GFFYGRGD or naphthalene-GFFYGRGE. The formation of supramolecular nanostructures improves the longitudinal relaxivity of the contrast agent up to 58.9 mM^{-1} s^{-1}. This large enhancement of the r_1 value could be applied *in vitro* for enzyme detection in aqueous solutions and cell lysates. In our opinion, these hydrogels may be very toxic *in vivo* because of the gadolinium ion loss owing to the peptide hydrolysis. In 2020, Accardo *et al.* developed novel supramolecular MRI diagnostic agents, based on the self-assembly of poly-aromatic peptide sequences.[73] These diagnostic agents [DTPA-PEG8-(FY)3 and DOTA-PEG8-(FY)3] contain two functional regions: a chelating agent (DTPA or DOTA), for the Gd^{3+} complexation, and a peptide-polymer [PEG8-(FY)3] able to form self-supporting and stable soft hydrogels at a concentration of 0.5–1.0% wt. Structural characterization suggested that the insertion of the chelating agent on the peptide building block sequence does not significantly change its aggregation properties. Indeed, both the peptide conjugates self-assemble into highly ordered tree-like multi-branch nanostructures, dominated by antiparallel β-sheet structures, and able to gelificate between 0.5 and 1.0% wt. According to the previously studied systems, relaxivity values of these fibrillary aggregates were found to be approximately 12 mM^{-1} s^{-1} at 20 MHz. Moreover, *in vitro* studies, on the metastasizing TS/A mouse mammary adenocarcinoma cell line, showed a good cytocompatibility of the nanostructures, even at high concentrations.

5. Nanogels

In recent years, researchers have turned their attention to new types of nanosized hydrophilic structures, to solve the problems associated with the use of Gd-based CAs in MRI studies. One of the proposed supramolecular systems is represented by hydrogel nanoparticles, usually named nanogels. These nanostructures are based on biocompatible polymers able to hold a large amount of water on their framework. These molecules can very quickly exchange with coordinated water increasing the relaxivity values per Gd complex embedded in the nanostructure. Moreover, inside these systems Gd-complexes are more stable, avoiding transmetallation reactions with endogenous ions, which are responsible for the toxicity of these CAs. Indeed, the release of Gd^{3+} ions has been related, in patients with impaired renal clearance values, to a very dangerous, and sometimes lethal, pathology called nephrogenic systemic fibrosis (NSF).[74] Moreover, a growing concern is derived from the evidence of a gradual accumulation of Gd^{3+} ions in the bones and in the brain of patients undergoing continuous administration of Gd-CAs over several years, even if they have normal renal clearance values.[75] The research has moved in different directions for the synthesis of these nanostructures. We can distinguish three main classes of nanogels: (i) nanogels in which the LMW Gd-complex is physically encapsulated; (ii) nanogels in which the Gd-complex is covalently bound, and (iii) nanogels in which the paramagnetic ion is used to prompt gel crosslinking. As expected, the relaxivity value of each nanosystem is strongly affected by the synthetic strategy used.

5.1 Gd complex encapsulated in nanogels

Gd-complexes can be directly encapsulated into nanogel structures. The first example of this was reported in 2011 by Keppler *et al.*,[76] who synthesized lectin-Gd-loaded CH nanogels with a prolonged clearance time. Tomato lectin (Lycopersicon esculentum agglutinin (LEA)) was chosen owing to its capacity to specifically bind the polysaccharide side chains of human endothelial cells. The LEA-DTPA conjugate was prepared by covalent coupling to the carboxyl groups of latex nanoparticles, and then complexed with gadolinium ions. LEA-DTPA-Gd conjugates were then encapsulated into CH hydrogel nanoparticles and assembled by the reverse microemulsion method. In order to evaluate the different loading capacities and MRI characteristics, spherical nanoparticles of different sizes (50–250 nm) were formulated by varying the concentrations of reactants. The large amount of Gd-DTPA encapsulated in a single nanosphere permits the detection of a strong MRI signal. Successively, in 2012 Chuburu *et al.* realized a new and straightforward formulation of gadolinium-loaded NPs, based on an ionotropic gelation process, for use as T1/T2 dual-mode contrast agents.[77] In this study, Gd-DOTA was encapsulated in CH/HA based nanoparticles, with a mean diameter between 235 and 284 nm. The release kinetics of the encapsulated CA, evaluated in PBS, detected no significant release after 3 d. The nanogels presented a r_1 and r_2 value of 72.3 and 177.5 mM^{-1} s^{-1} respectively, at a concentration of 1 mM and at 60 MHz. *In vitro* studies were carried out to measure the mitochondrial enzyme activity of C6 glioma cells, and showed no nanoparticle toxicity even at high concentrations. Two years later, the same research group tuned the composition of the previously synthesized Gd-NPs. They also compared two different approaches to incorporate Gd-CAs by physical gelation within CH-NPs.[78] According to the first procedure, CH-NPs were constituted of a single polymer network incorporating Gd-DOTP or MS325. In the second protocol, CH-NPs were composed of a hybrid polymer network (CH, solubilized in a citric acid solution, was left to react with HA and sodium tripolyphosphate, TPP). The formation of the polyelectrolyte complexes induced the gelation process; then Gd-DOTP or MS325 was incorporated into the polyanion phase. Relaxivity studies highlighted enhancements in both the r_1 and

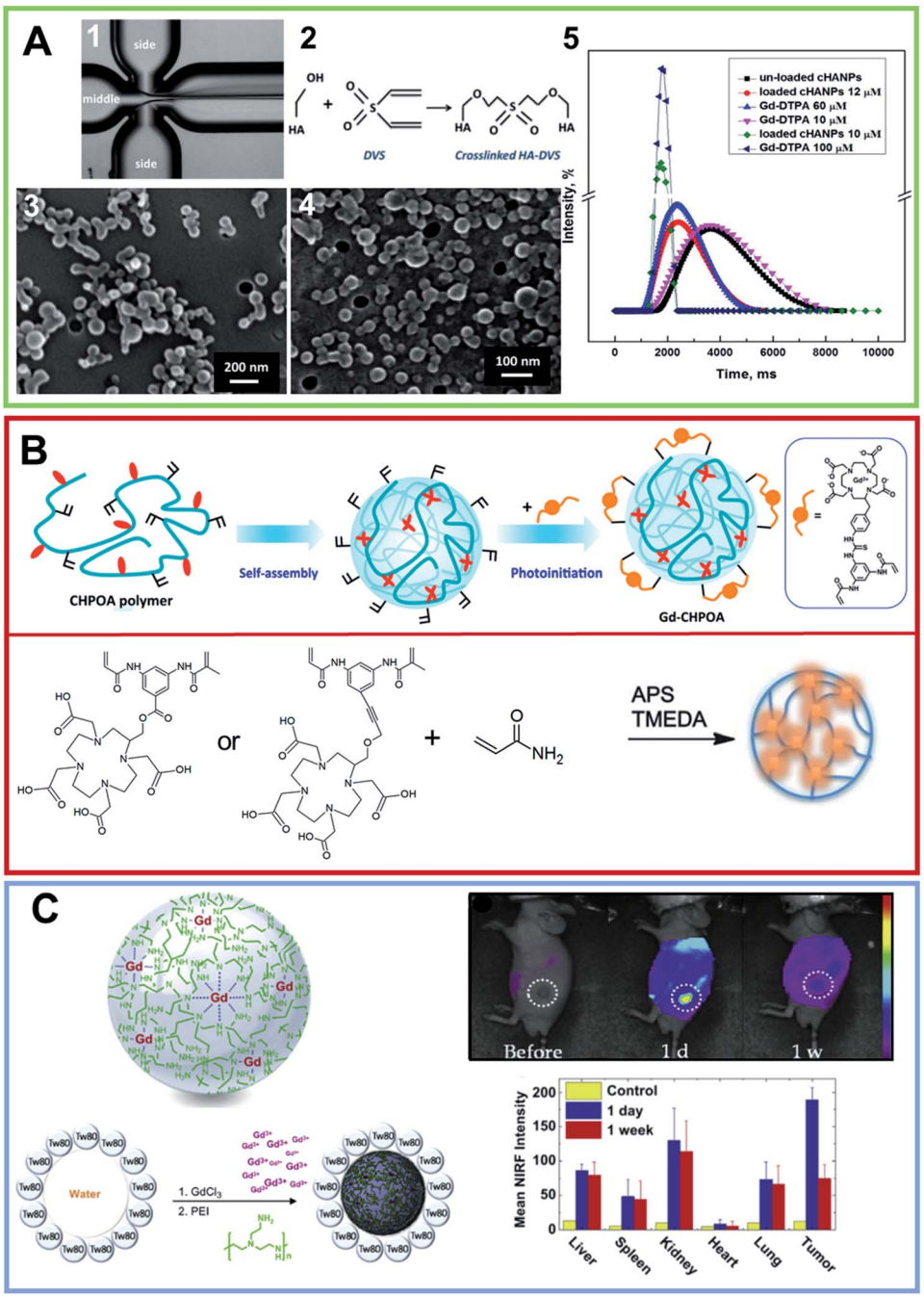

Fig. 6 (A) (1) Optical fluorescence microscopy photo of flow-focusing pattern used for obtaining the nanogel formulation using a microfluidic approach. (2) Schematic crosslinking reaction involving HA hydroxyl groups with DVS. FE-SEM images of crosslinked HA nanoparticles (cHANPs) in aqueous solution in (3) 0.8% v/v of DVS added in the middle channel and (4) 4% v/v of DVS added in the side channels. (5) *In vitro* relaxation time distribution reported for: Gd-DTPA in water solution at (purple line) 10 μmol L^{-1}, (light blue line) 60 μmol L^{-1} and (blue) 100 μmol L^{-1}; un-loaded cHANPs (black line). Also reported are the loaded HA nanoparticles at standard conditions obtained using (red line) 4% v/v DVS in the side channels, at pH 12.3, reported at 12 μmol L^{-1} of Gd-DTPA, (green line) 0.8% v/v DVS and Cspan80 tensioactive 0.5% v/v in the middle channel, reported at Gd-DTPA of 10 μM (reproduced with permission[83]). (B) Upper row, nanogel formulation obtained by self-assembling of a cholesterol and acryloyl-modified polysaccharide pullulan (CHPOA). The photoinduced crosslinkage of the acryloyl groups on the nanogel surface of the DOTA-Gd modified chelating agent (GdCHPOA) allows the creation of T1 MRI contrast agents (adapted with permission,[89] copyright 2015-American Chemical Society). Lower row: chemical structure of two macrocyclic DOTA-based crosslinkers. Polymers were converted in polyacrylamide-based nanogels using an inverse emulsion process *via* ammonium persulfate (APS) as the initiator and by adding tetramethylethylenediamine (TMEDA) to control the radical polymerization rate (arranged from ref. 88. Reproduced by permission of The Royal Society of Chemistry). (C) Graphical representation of the functional metal–organic coordinated nanogels (GdNGs) obtained using the branched poly(ethyleneimine) (PEI) polymer *via* the colloidal reverse microemulsion method. On the right, *in vivo* NIRF images of the SCC7 tumor-bearing mouse before and after tail vein injection (1 d and 1 week) of the GdNGs and the biodistribution of the GdNGs, obtained by NIRF signals from the dissected organs and tumors before (control) and after injection (reproduced with permission[93]).

r_2 values. They appeared to be more important for Gd-DOTP, indicating that the first sphere relaxation effects provide a minor contribution to the relaxivity enhancement, which is mainly ruled by the second sphere contribution. Indeed, the gain in relaxivity was more important for hydrogels that corresponded to the hybrid polymer network, owing to the high number of water molecules involved in the network. These results indicated a direct relationship between the relaxivity performance and the hydrogel matrix composition. Finally, *in vitro* studies showed no toxicity against primary fibroblast cells, in accordance with the results of the MTT assay. Later, the same group also designed and synthesized CH/TPP/HA nanohydrogels loaded with gadolinium complexes, for long-term MRI of lymph nodes (LNs).[79] These Gd-DOTA loaded nanohydrogels were prepared according to the previously employed ionotropic gelation process. In order to obtain NPs with a diameter of less than 100 nm, able to be drained to LNs, CH with molecular weights of 51 kDa (CH51) and 37 kDa (CH37) were used. Beyond the molecular weight of CH, for the formulations the authors also varied several experimental conditions such as the nature of the acid (citric/acetic acid) used for CH solubilization and the CH/TPP ratio (from 0.5 to 12), whereas the HA concentration was kept constant. The results highlighted that the decrease of the CH molecular weight, as well as the CH/TPP ratio, did not induce a decrease in the nano-object size, but only the nanoparticle density in the nanosuspensions (the low CH/TPP led to an increase in the particle density). Moreover, the results indicated the effect of the different acids on the number of formed nanoparticles. Therefore, the amount of Gd-DOTA encapsulated inside nanohydrogels was reduced when using LMW CH. The relaxivity measurements of the resulting nanomaterials indicated their good ability to increase the r_1 longitudinal relaxation rates and the MRI efficiency at 1.5 T. Preliminary cytotoxicity studies, on the SVEC4-10 murine lymph node endothelial cell line, highlighted the good biocompatibility of the nanohydrogels. Very recently, Dinischiotu *et al.*, in collaboration with Chuburu's group, thoroughly investigated the biocompatibility of these CH/TPP/HA nanogels prepared at two different concentrations of CH (2.5 and 1.5 mg mL^{-1}) and loaded with Gd-DOTP or Gd-DOTA complexes.[80] Quantification of the gadolinium ions highlighted the better loading capability of the formulations containing 2.5 mg mL^{-1} of CH. The CH concentration, type of acid or gadolinium contrast agent did not affect the cell survival profiles and the LDH release in SVEC4-10 murine lymph node endothelial cells. Moreover, none of the tested nanogels induced changes in the Nrf-2 protein expression. Another example of CH nanoparticles conjugated with gadolinium *meso*-tetrakis(4-pyridyl)porphyrin [Gd(TPyP)] was described in 2015 by Korri-Youssoufi *et al.*[81] In this study, nanogels were prepared by ionic gelation using bulk LMW and medium molecular weight (MW) CH with different degrees of deacetylation. Gd(TPyP) loaded CH nanoparticles were realized *via* passive absorption by adding various quantities of Gd(TPyP) to CH nanoparticles. The longitudinal and transverse relaxivities of the Gd(TPyP) nanoparticles in aqueous solution have been evaluated, showing a value of 38.35 mM^{-1} s^{-1} for r_1, higher than that of free Gd(TPyP) and commercial Gd-DOTA. On the other hand, the r_2 value in water was found to be 33.43 mM^{-1} s^{-1}, lower compared with free Gd(TPyP), this is probably due to the greater solubility of the compound in water.

In 2018 Ardestani *et al.* reported the synthesis and characterization of a new theranostic CH-carbon dot quantum hybrid nanogel functionalized with dimeglumine gadopentetate.[82] The preparation of the nanoparticles, with an average size of 140 nm, was achieved by adding CH, EDTA and finally glutaraldehyde in sequence, to carbon quantum dots. *In vitro* studies, using normal kidney, HEK-293 and MCF-7 breast cell lines, demonstrated the ability of the nanogel-drug to enter the cell, which appears to be five times more likely than the drug alone, especially for HEK-293. According to the MTT assay and the apoptosis–necrosis test, the nanogel showed less toxicity than the free drug.

PCR quantitative analysis revealed an increase in the Bcl-2 gene expression, followed by a decrease in the Bax expression on the MCF-7 cell line. In addition to several examples of nanogels prepared using the ionotropic gelation process, nanogels can be prepared using a microfluidic flow-focusing platform.[83] In this approach crosslinked HA nanogels entrapping Gd-DTPA were synthesized using divinyl sulfone (DVS) as a crosslinking agent.[83,84] DVS was alternately injected into the middle microfluidic channel or into the side channels and the role played by the concentration, pH and hydrophilic–lipophilic balance (HLB) of the selected surfactants was monitored (Fig. 6A). An increase in the DVS concentration (from 0.6 to 1% v/v) enabled an increase in the encapsulation efficiency and loading capability of the resulting nanoparticles. In the second approach, smaller nanoparticles (~40 nm) were formed, under standard flow conditions and at a pH equal to 12.3, by adding DVS up to 4% v/v to the side channels. Optimizing the process parameters and the crosslinking reaction, a T1 of 1562 mM^{-1} s^{-1} was achieved with 10 μM of the Gd-loaded nanoparticles suspension. A year later, the same group described a process that could be used to produce nanoparticles, encapsulated with both Gd-DTPA and a dye for dual imaging applications. The nanoparticles presented a CH core and an outer shell of HA, consisting of double crosslinking obtained using TPP and DVS.[85] The crosslinkers were used in reverse, specifically TPP to the coacervant phase and DVS to the aqueous phase. Different gradients of temperature were tested and the pH was controlled and kept at a value ranging from 4.5–5 to minimize the time of the coacervation step. Stability studies, performed at various pH values, highlighted the peculiar and interesting pH-sensitive behavior of the nanovectors. MRI studies showed that, during the crosslinking, a relaxation rate T1 of 1720 ms was achieved for a suspension of 20 μM of Gd-loaded nanoparticles. *In vitro* cytotoxicity studies on the adenocarcinoma human alveolar basal epithelial cell line (A549) revealed that, in a range between 200 and 100 μg mL^{-1}, the nanoparticles showed no detectable toxicity. Several specific dyes, Cy5, Atto 633, FITC, were alternately added to the aqueous phase at concentrations ranging from 0.1 to 1 mg mL^{-1} for *in vivo* optical imaging. Gd-loaded nanoparticles appeared capable of maintaining their cargo of CA, and therefore their boosted relaxometric properties.

Wu *et al.* designed and synthesized thermally responsive hydrogel–lipid-hybrid nanoparticulate (HLN), in which stable Gd-hydrogel nanoparticles were loaded into a solid lipid nanoparticle matrix that prevented T1-weighted contrast signal enhancement. Poly(*N*-isopropylacrylamide-coacrylamide) (NIPAM-*co*-AM) nanogels (with a mean diameter lower than 15 nm) were prepared using bisallylamidodiethylenetriaminetriacetic acid, a novel crosslinker able to chelate Gd(III) ions.[86] This supramolecular aggregate provides a very innovative application as a thermometric window for the Gd(III) hydrogel. Increasing the temperature, the melting of the matrix lipid releases the Gd-hydrogel nanoparticles, enhancing the contrast signal. When the temperature was further raised above the volume phase transition temperature of the hydrogel nanoparticles, they collapsed and provided an 'on–off' signal diminution. Both the 'off–on' and the 'on–off' transition temperature could be tuned by changing the lipid matrix and altering the NIPAM/AM ratio in the hydrogel, respectively.

5.2 Covalently bound Gd complexes

Gd-complexes can also be covalently bound on the nanogel, as an alternative. The chemical anchorage of the Gd-complex on the nanogels can occur in distinct ways. One of the simplest strategies is the design and synthesis of a Gd-complex containing a monomer able to generate nanogels under specific experimental self-assembling conditions. Another strategy, is based instead on the employment the gadolinium complexes directly as crosslinker agents during the generation of nanogels. This strategy allows the entire nanoparticle to incorporated into the CA, keeping the nanogel surface available for functionalization with other compounds (for example with targeting molecules). Alternatively, the preparation of the Gd-nanogel can be achieved by covalently binding the metal complex onto the nanogel after preparation. A summary of the nanogels prepared by using these approaches and their structural and relaxometric properties are reported in Table 2. According to the first strategy, based on the self-assembly of a Gd-complex containing monomer, in 2015, Zhu *et al.* synthesized nanospheres based on a derivative of HA functionalized with a DTPA(Gd) complex (HA-Gd-DTPA) as a novel lymphatic system.[87] The self-assembled HA-Gd-DTPA nanospheres exhibited an average hydrodynamic size of around 300 nm. The relaxivity studies showed that the nanoformulation led to a r_1 value of 11.35 mM^{-1} s^{-1} when measured using a 3 T MRI scanner. Preliminary *in vitro* studies, performed on L929 cells, indicated a cell viability of around 90% for cells incubated for 12 h at a dose of 1.5 mg mL^{-1}. Moreover, *in vivo* studies on rabbits demonstrated that the nanospheres had a lymphographic effect superior to that of Magnevist®. Thanks to their dimensions and targeting capabilities, these nanostructures could be used as lymphatic system-specific CAs. Using a completely different strategy, in which the gadolinium complexes (*e.g.* DTPA or DOTA) act as crosslinker agents in the generation of nanogels, Almutairi *et al.* formulated three nanogels of polyacrylamide (PAA).[88] In detail, they synthesized one crosslinker starting from the DTPA chelating agent and two others crosslinkers starting from DOTA. After coordination with gadolinium, the three crosslinker agents [1Gd(III), 2Gd(III) and 3Gd(III)] were used to prepare the PAA/1Gd(III), PAA/2Gd(III) and PAA/3Gd(III) nanogels, through the inverse emulsion process (Fig. 6B). As expected, the obtained nanogels, with a mean diameter ranging between 50 and 85 nm, allowed prolonged circulation and were found to be thermodynamically and kinetically more inert than Magnevist® *versus* transmetallation with Zn^{2+} in phosphate buffer. The incorporation of 1Gd(III) into the PAA based nanogels allowed an increase in the relaxivity up to 9.7 mM^{-1} s^{-1} at 60 MHz and 37 °C. In the same way, the DOTA-based crosslinkers 2Gd(III) and 3Gd(III) showed higher relaxivities than Dotarem® (4.3 and 5.0 mM^{-1} s^{-1} respectively, at 60 MHz and 37 °C), and the nanogels formed revealed an increase in the r_{1p} values up to 17.6 and 14.8 mM^{-1} s^{-1}, respectively. The increase in relaxivity probably depends on the rigidity of the system after crosslinking. Nevertheless, the interesting relaxometric properties of these nanogels, their formulation, and the use of *in situ* on emulsion polymerization, was not highly reproducible. Moreover, the surfactants required for their preparation are difficult

Table 2 Gadolinium complex, synthetic approach used to prepare nanoparticle hydrogels, mean diameter of nanogels, relaxivity value at a 1 mM concentration and references

System	Gd(III) complex	Synthetic approach	Mean diameter (nm)	r_{1p} (mM^{-1} s^{-1})	# ref.
HA-Gd-DTPA	Gd-DTPA	Self-assembly of the Gd-derivative	300	11.4[a]	87
PAA/1Gd(III)	Gd-DTPA	Inverse emulsion using Gd-complex as crosslinker	$50 < d < 85$	9.7[b]	88
PAA/2Gd(III)	Gd-DOTA			17.6	
PAA/3Gd(III)	Gd-DOTA			14.8	
Gd-CHPOA	Gd-DOTA	Photoinitiation using Gd-complex as crosslinker	65	24.1[b]	89
POEMA/AEMA/EGDMA	Gd-DTPA	Free radical polymerization and post-functionalization with Gd-complex	10	20.8[c]	90
VCL/VOU	NH_2-DOTA(Gd)-GA	Precipitation and post-functionalization with Gd-complex	180	6.85[c]	91
Dex-PGMA	Gd-DTPA	Graft polymerization and post-functionalization Gd-complex	185	44.4[a]	92

[a] The relaxivity value was recorded at 3.0 T. [b] The relaxivity value was recorded at 1.41 T. [c] The relaxivity value was recorded at 0.5 T.

to remove. To overcome these drawbacks, in 2015 the same authors explored an alternative synthetic approach based on photoinitiation.[89] In this procedure, a cholesterol and acryloyl-modified polysaccharide pullulan (CHPOA) polymer, characterized by a high biocompatibility, and an ability to self-assemble into nanogels through hydrophobic interactions amongst the cholesterol moieties was formulated. Then, thanks to the photoinitiation, Gd-chelating DOTA crosslinkers were reacted with the acryloyl groups (Fig. 6B). The resulting nanogels, having a mean diameter of 65 nm, present a high colloidal and high Gd-chelating stability. Moreover, they have a longitudinal (T1) relaxivity value (24.1 mM^{-1} s^{-1} at 1.41 T) that is higher than the nanogels previously obtained. These Gd-chelating pullulan nanogels (Gd-CHPOA) caused no organ dysfunction for up to 3 months after intravenous injection in mice.

Beyond the crosslinking approach, there are three examples in the literature of Gd-nanogels obtained using a post-functionalization method in which the Gd-complex is covalently bound on the preformed nanogel. The first example in this direction was reported by Gillies *et al.* in 2013.[90] They obtained very small nanogels, with a mean diameter of 10 nm, using a free radical polymerization approach by starting from poly(ethylene glycol) methyl ether methacrylate (POEMA) and *N*-(2-aminoethyl) methacrylamide hydrochloride (AEMA) as monomers for the preparation. Moreover, ethylene glycol dimethacrylate (EGDMA) was used as a crosslinking agent and benzoyl peroxide was employed as an initiator. POEMA was selected by the authors owing to its hydrophilicity, it should provide a significant enhancement in the water accessible to the nanogel, and in turn increase the relaxivity value of the nanosystem. Moreover, the pendant amine functionalities on AEMA were derivatized with an isothiocyanate derivative of DTPA and, finally, gadolinium coordination was achieved. The obtained nanogel had r_1 values of 20.8 and 17.5 mM^{-1} s^{-1} at 20 and 60 MHz, respectively. The nanogel, injected in mice, showed an enhanced contrast and vascular circulation compared to Magnevist®. Later, a new example of a nanogel for MRI purposes was prepared by Shi *et al.* by post-functionalizing poly(*N*-vinylcaprolactam) (VCL) nanogels with the DOTA(Gd) derivative, NH_2-DOTA(Gd)-GA.[91] In the first step the authors achieved the synthesis of the nanogel *via* precipitation polymerization of VCL with acrylic acid (Aac) and with the degradable crosslinker 3,9-divinyl-2,4,8,10-tetraoxaspiro-[5,5]-undecane (VOU). Then, the surface of the PVCL nanogels was covalently modified with the Gd-complex on the carboxylic groups. The size distributions of the nanogel before and after modification with NH_2-DOTA(Gd)-GA did not show any significant differences and had an average diameter around 180 nm. Relaxivity values, at different gadolinium concentrations, were constants with an average r_1 value of 6.85 mM^{-1} s^{-1} measured with a 0.5 T MRI scanner. Moreover, viability assays carried out on HeLa cells treated with PVCL-Gd nanogels (NGs) with various Gd loadings (10–300 μM), demonstrated the good cytocompatibility of the formulation, with a cell viability of more than 70%. Finally, the PVCL-NGs were found to be able to enhance the MR imaging of cancer cells and of subcutaneous tumor models *in vivo* with an increase in the MR signal-to-noise ratio (SNR) compared to Magnevist®. In the same year, Dou *et al.* synthesized dextran-poly(glycidyl methacrylate) (Dex-PGMA) nano-suitcases *via* a graft copolymerization induced self-assembly (GISA) approach.[92] Then, these nano-suitcases were modified with hydrazine groups in order to afford non-covalent interactions between the hydrazine group and the carboxylic groups of Gd-DTPA. The amount of the Gd-complex in the nano-suitcases, estimated using inductively coupled plasma atomic emission spectroscopy (ICP-AES), was 22.6% wt. The dimensions of the Dex-PGMA-Gd(III) hybrid nanosystems (~185 nm in aqueous solution) are suitable for lymph node accumulation. Moreover, the obtained nanostructure had a very high value of relaxivity, with a r_1 and r_2 relaxivity values of 44.4 and 9.54 mM^{-1} s^{-1} at 3.0 T. Owing to the low r_2/r_1 ratio (~0.21), the Dex-PGMA-Gd(III) nano-suitcases can be considered as potentially positive CAs. As expected, based on their dimensions, these aggregates were found to be able to accumulate the Gd-complex *in vivo* in the lymph nodes of rats and provide strong MR-signals.

5.3 Crosslinked by Gd ions

Gadolinium or others paramagnetic ions, such as manganese, were also directly used as crosslinker agents during nanogel formation. For example, Kim *et al.* developed Gd^{3+} ions coordinated to branched PEI nanogels (GdNGs).[93] The non-crystalline elastic polymer nanogel, that was randomly crosslinked was obtained by mixing the PEI chains with Gd^{3+} ions in aqueous solution (Fig. 6C). Owing to random crosslinking of flexible polymer chains, the resulting nanogel presents an irregular gelation with the core and overall hydrodynamic sizes of approximately 65 and 160 nm and a high elasticity, with an apparent Young's modulus of 3.0 MPa. In contrast to common T1-enhancing gadolinium complexes, Gd-NGs showed the capability of enhancing the negative T2 contrast (r_2 = 82.6 mM^{-1} s^{-1}). Gd-NGs manifested strong intracellular entry into SCC7 (squamous cell carcinoma) cells with no apparent toxicity, suggesting that toxic Gd^{3+} ions are solidly trapped in the PEI network. Owing to their features, these nanogels showed a long blood circulation time as opposed to the rapid system clearance of common nanohybrids that usually undergo sequestration and filtration by the RES. *In vivo* studies, carried out in mice, demonstrated efficient systemic targeting and dual-modality (magnetic resonance/fluorescence) visualization of the tumor area (Fig. 6C). Successively, in 2017 Warszyński *et al.* synthesized another example of a theranostic nanogel, in which alginate gel nanoparticles have been prepared using the reverse microemulsion and physical crosslinking method prompted by Gd(III) ions.[94] The nanogel surface was then modified using the layer-by-layer (LbL) technique using natural polyelectrolytes: CH as the polycation with a zeta potential (ζ) value of +45 mV and alginate (ALG) as the polyanion with ζ −35 mV. The structural characterization of the LbL modified Gd-NG (5 layers) determined the average size and a ζ value of 110 nm and −30 mV, respectively in a 0.015 M NaCl solution. *In vitro* studies indicated that no statistically significant toxic effects were found for both the non-modified and LbL modified nanogels on

the human neuroblastoma cell line SH-SY5Y. Moreover, Gd-NGs were found able to significantly reduce the T1 relaxation time relative to the control samples. At the same time, Leal *et al.* synthesized a highly efficient crosslinked NG based on another paramagnetic ion, the manganese, incorporated into a pH sensitive polymeric hydrogel matrix, composed of 4-vinylpyridine (4-VP) and divinylbenzene (DVB) monomers.[95] The Mn chelate nanogel switches on as a dual MRI contrast agent upon a change in the pH, being able to produce both positive and negative contrast on T1- and T2-weighted MR images. The relaxivities, r_2 and r_1, for the Mn-NG at pH 3.8 were 19.6 and 10.6 mM^{-1} s^{-1}, respectively, at a low magnetic field (1.5 T). This nanoswitch presents the characteristics of a T1 CA with an r_2/r_1 ratio of 1.8. In contrast, at a high magnetic field (9.4 T), the hydrogel behaves as a T2 CA with relaxivity values of 306.3 and 14.6 mM^{-1} s^{-1}, respectively. *In vitro* studies, carried out on the rat glioma cell line C6 cell, showed a high viability with a cell survival value of above 80%.

6. Conclusion

Magnetic resonance imaging CAs based on Gd-complexes are employed in approximately 40% of clinical examinations used to visualize small tumor lesions. Even if highly accurate, MRI modality suffers because of its low sensitivity and LMW-CAs rapidly extravasate after their administration. For these reasons, in the last two decades many macro- and supramolecular multimeric gadolinium complexes (dendrimers, polymers, carbon nanostructures, micelles and liposomes) have been designed to increase their performance and to reduce the administered dose. One of the most promising applications of these nanostructures is the possibility of combining two or more diagnostic agents. In this context, in recent years several examples of nanoparticles have been proposed for simultaneous visualization using different diagnostic techniques.[96–98] However, research on novel supramolecular systems such as fibers, hydrogels and nanogels has become particularly relevant after the European Medicines Agency (EMA) decided to withdraw contrast agents based on linear chelators from the market as they were considered to not be sufficiently stable in relation to the *in vivo* release of toxic Gd(III) ions. Supramolecular systems have been identified as innovative vehicles for CAs that are able to significantly increase their relaxivity values. Indeed, it was observed that nanogels that encapsulate LMW-CAs have very high relaxivity values (up to 100 mM^{-1} s^{-1}). On the other hand, it can be observed that nanostructures in which the Gd-complex is covalently bound exhibit lower relaxivity values. The reasons for these differences, in terms of the performance, are not yet completely clear. The availability of high-relaxivity nanosystems could provide the answer to the urgent need for reducing the clinical dose. This strategy could allow long-term adverse health effects to be minimized owing to the *in vivo* metal deposition. Moreover, the capability of the supramolecular nanostructures to shield Gd-complexes from transmetallation reactions may prevent unwanted biotransformation, which are the basis of *in vivo* metal accumulation. Obviously, the preparation and exploitation of these supramolecular Gd-CAs is not trivial. For this reason, this strategy should be the preferred method only if it is strictly necessary. Identification of the structural parameters that affect the performance of the supramolecular CA could allow novel soft materials to be designed for use in the clinic in the future.

7. Methodology

A systematic literature review was performed according to PRISMA (Preferred Reporting Items for Systematic Reviews and Meta-Analyses) criteria. Scientific contributions were critically selected *via* consecutive operations, related to identification, screening, eligibility and inclusion steps (see Scheme 1). Published studies were correlated to the selected topic and were identified using an electronic search in SciFinder Scholar web database, that includes PubMed, Caplus and Medline. A systematic literature review was performed using English keywords and refining procedures were applied. The operators "OR" and "AND" were used in order to obtain an inclusive and restrictive outcome. SciFinder Scholar web database was first questioned using the "MRI contrast agent" query, producing 14 012 results. A consecutive refinement with "gadolinium" produced 5610 outcomes. Removing duplicates, non-English languages, and selecting only journal, review book and letter contributions, gradually decrease the number of results from 4474 to 4105, and finally to 3514. These latter outcomes were further analyzed using the following keywords: fiber (29 results), hydrogel (21 results), hydrogel nanoparticle (10 results), nanogel (6 results), nanohydrogel (2 results), and chitosan nanoparticles (42 results). The articles related to CEST contrast agents, nanocomposites, micelles and gadolinium oxide were excluded. A manual search in the reference list of the eligible products was performed in order to identify additional relevant

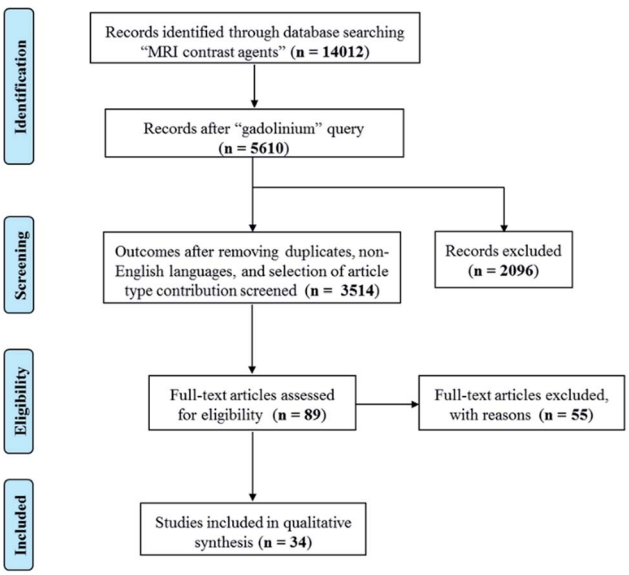

Scheme 1 Scheme describing the systematic literature review performed according to PRISMA (Preferred Reporting Items for Systematic Reviews and Meta-Analyses) criteria.

papers, in case they were missed in the online searches. The clear identification of the relevant literature data was performed including the title, abstract and full-text reading procedures. The research provided 9 results about fibers, 14 regarding hydrogels and 20 about nanogels.

Conflicts of interest

There are no conflicts to declare.

Acknowledgements

This work was supported by the PRIN-2017A2KEPL project and by the grant from Regione Campania-POR Campania FESR 2014/2020 "Combattere la resistenza tumorale: piattaforma integrata multidisciplinare per un approccio tecnologico innovativo alle oncoterapie-Campania Oncoterapie" (Project No. B61G18000470007).

Notes and references

1 A. R. Kherlopian, T. Song, Q. Duan, M. A. Neimark, M. J. Po, J. K. Gohagan and A. F. Laine, *BMC Syst. Biol.*, 2008, **2**, 74–92.
2 R. Salzer, *Biomedical imaging: principles and applications*, John Wiley & Sons, Inc., Hoboken, NJ USA, 2012.
3 E. C. Lin, *Mayo Clin. Proc.*, 2010, **85**, 1142–1146.
4 J. A. Seibert and R. L. Morin, *Pediatr. Radiol.*, 2011, **41**, 573–581.
5 F. A. Gallagher, *Clin. Radiol.*, 2010, **65**, 557–566.
6 A. Ng and J. Swanevelder, *Cont. Educ. Anaesth. Crit. Care Pain*, 2011, **11**, 186–192.
7 N. Ji, *Neuron*, 2014, **83**, 1242–1254.
8 S. K. Nune, P. Gunda, P. K. Thallapally, Y. Y. Lin, M. Laird Forrest and C. J. Berkland, *Expert Opin. Drug Delivery*, 2009, **6**, 1175–1194.
9 M. A. Farrukh, *Functionalized nanomaterials*, InTech-Open Access Publisher, London, UK, 2016.
10 T. H. LaBean, *Nature*, 2009, **459**, 331–332.
11 A. P. Khandhar, P. Keselman, S. J. Kemp, R. M. Ferguson, P. W. Goodwill, S. M. Conolly and K. M. Krishnan, *Nanoscale*, 2017, **9**, 1299–1306.
12 X. Huang, R. O'Connor and E. A. Kwizera, *Nanotheranostics*, 2017, **1**, 80–102.
13 R. Cheheltani, R. M. Ezzibdeh, P. Chhour, K. Pulaparthi, J. Kim, M. Jurcova, J. C. Hsu, C. Blundell, H. I. Litt, V. A. Ferrari, H. R. Allcock, C. M. Sehgal and D. P. Cormode, *Biomaterials*, 2016, **102**, 87–97.
14 I. R. Young, *Methods in biomedical magnetic resonance imaging and spectroscopy*, John Wiley & Sons, Inc., Chichester, UK, 2012.
15 P. A. Rinck, *Magnetic resonance in medicine*, ABW Wissenschaftsverlag GmbH, Berlin, Germany, 2003.
16 V. C. Pierre and M. J. Allen, *Contrast agents for MRI: experimental methods*, RSC, Croydon, UK, 2018.
17 A. Merbach, L. Helm and E. Toth, *The chemistry of contrast agents in medical magnetic resonance imaging*, John Wiley & Sons, Inc., Hoboken, NJ USA, 2013.
18 S. Laurent, C. Henoumont, D. Stanicki, S. Boutry, E. Lipani, S. Belaid, R. N. Muller and L. V. Elst, *MRI Contrast agents: from molecules to particles*, Springer, Singapore, 2017.
19 C. Corot and D. Warlin, *Wiley Interdiscip. Rev.: Nanomed. Nanobiotechnol.*, 2013, **5**, 411–422.
20 S. Aime, E. Gianolio and A. Viale, in *Paramagnetism in experimental biomolecular NMR*, ed. C. Luchinat, G. Parigi and E. Ravera, RCS, Cambridge, UK, 2018, pp. 189–218.
21 P. Caravan, N. J. Cloutier, M. T. Greenfield, S. A. McDermid, S. U. Dunham, J. W. Bulte, J. C. Amedio Jr, R. J. Looby, R. M. Supkowski, W. D. Horrocks Jr, T. J. McMurry and R. B. Lauffer, *J. Am. Chem. Soc.*, 2002, **124**, 3152–3162.
22 A. W. Bosman, H. M. Janssen and E. W. Meijer, *Chem. Rev.*, 1999, **99**, 1665–1688.
23 D. L. Ladd, R. Hollister, X. Peng, D. Wei, G. Wu, D. Delecki, R. A. Snow, J. L. Toner, K. Kellar, J. Eck, V. C. Desai, G. Raymond, L. B. Kinter, T. S. Desser and D. L. Rubin, *Bioconjugate Chem.*, 1999, **10**, 361–370.
24 C. Diaferia, E. Gianolio and A. Accardo, *J. Pept. Sci.*, 2019, **25**, 3157.
25 T. S. Desser, D. L. Rubin, H. Muller, G. L. McIntire, E. R. Bacon and K. R. Hollister, *Acad. Radiol.*, 1999, **6**, 112–118.
26 A. Dirksen, S. Langereis, B. F. M. de Waal, M. H. P. van Genderen, T. M. Hackeng and E. W. Meijer, *Chem. Commun.*, 2005, 2811–2813.
27 S. Aime, E. Gianolio, E. Terreno, I. Menegotto, C. Bracco, L. Milone and G. Cravotto, *Magn. Reson. Chem.*, 2003, **41**, 800–805.
28 B. Sitharaman and L. J. Wilson, *J. Biomed. Nanotechnol.*, 2007, **3**, 342–352.
29 P. P. Fatouros and M. D. Shultz, *Nanomedicine*, 2013, **8**, 1853–1864.
30 R. Sethi, Y. Mackeyev and L. J. Wilson, *Inorg. Chim. Acta*, 2012, **393**, 165–172.
31 K. B. Hartman, S. Laus, R. D. Bolskar, R. Muthupillai, L. Helm, E. Toth, A. E. Merbach and L. J. Wilson, *Nano Lett.*, 2008, **8**, 415–419.
32 A. Accardo, D. Tesauro, L. Aloj, C. Pedone and G. Morelli, *Coord. Chem. Rev.*, 2009, **253**, 2193–2213.
33 E. Cittadino, M. Botta, L. Tei, F. Kielar, R. Stefania, E. Chiavazza, S. Aime and E. Terreno, *ChemPlusChem*, 2013, **78**, 712–722.
34 G. Lipari and A. Szabo, *J. Am. Chem. Soc.*, 1982, **104**, 4546–4559.
35 G. Lipari and A. Szabo, *J. Am. Chem. Soc.*, 1982, **104**, 4559–4570.
36 T. Fan, X. Yu, B. Shen and L. Sun, *J. Nanomater.*, 2017, **9**, 1–16.
37 Y. Wang, J. Chou, Y. Sun, S. Wen, S. Vasilescu and H. Zhang, *Mater. Sci. Eng., C*, 2019, **101**, 650–659.
38 J. J. Panda and V. S. Chauhan, *Polym. Chem.*, 2014, **5**, 4418–4436.
39 D. Tesauro, A. Accardo, C. Diaferia, V. Milano, J. Guillon, L. Ronga and F. Rossi, *Molecules*, 2019, **24**, 351–378.
40 A. Ghosh, M. Haverick, K. Stump, X. Yang, M. F. Tweedle and J. E. Goldberger, *J. Am. Chem. Soc.*, 2012, **134**, 3647–3650.

41 C. Diaferia, E. Gianolio, P. Palladino, F. Arena, C. Boffa, G. Morelli and A. Accardo, *Adv. Funct. Mater.*, 2015, **25**, 7003–7016.
42 C. Diaferia, E. Gianolio, A. Accardo and G. Morelli, *J. Pept. Sci.*, 2017, **23**, 122–130.
43 M. Reches and E. Gazit, *Science*, 2003, **300**, 625–627.
44 C. Diaferia, F. A. Mercurio, C. Giannini, T. Sibillano, G. Morelli, M. Leone and A. Accardo, *Sci. Rep.*, 2016, **6**, 26638.
45 C. Diaferia, E. Gianolio, T. Sibillano, F. A. Mercurio, M. Leone, C. Giannini, N. Balasco, L. Vitagliano, G. Morelli and A. Accardo, *Sci. Rep.*, 2017, **7**, 307–321.
46 C. Diaferia, N. Balasco, T. Sibillano, M. Ghosh, L. Adler-Abramovich, C. Giannini, L. Vitagliano, G. Morelli and A. Accardo, *Chem.–Eur. J.*, 2018, **24**, 6804–6817.
47 J. Huang, C. L. Hastings, G. P. Duffy, H. M. Kelly, J. Raeburn, D. J. Adams and A. Heise, *Biomacromolecules*, 2013, **14**, 200–206.
48 I. Kim, E. H. Han, J. Ryu, Y. J. Min, H. Ahn, Y. H. Chung and E. Lee, *Biomacromolecules*, 2016, **17**, 3234–3243.
49 J. Zhang, Y. Mu, Z. Ma, K. Han and H. Han, *Biomaterials*, 2018, **182**, 269–278.
50 I. Kim, S. Jin, E. Han, E. Ko, M. Ahn, W. Bang, J. Bang and E. Lee, *Biomacromolecules*, 2017, **18**, 3600–3610.
51 L. M. Randolph, C. L. M. LeGuyader, M. E. Hahn, C. M. Andolina, J. P. Patterson, R. F. Mattrey, J. E. Millstone, M. Botta, M. Scadeng and N. C. Gianneschi, *Chem. Sci.*, 2016, **7**, 4230–4236.
52 J. Radhakrishnan, A. Subramanian, U. M. Krishnan and S. Sethuraman, *Biomacromolecules*, 2017, **18**, 1–26.
53 A. Dasgupta, J. H. Mondal and D. Das, *RSC Adv.*, 2013, **3**, 9117–9149.
54 R. Langer and J. P. Vacanti, *Science*, 1993, **260**, 920–926.
55 J. Li and D. J. Mooney, *Nat. Rev. Mater.*, 2016, **1**, 16071.
56 A. Berdichevski, H. S. Yameen, H. Dafni, M. Neeman and D. Seliktara, *Proc. Natl. Acad. Sci. U. S. A.*, 2015, **112**, 5147–5152.
57 J. Liu, K. Wang, J. Luan, Z. Wen, L. Wang, Z. Liu, G. Wu and R. Zhuo, *J. Mater. Chem. B*, 2016, **4**, 1343–1353.
58 D. Bermejo-Velasco, W. Dou, A. Heerschap, D. Ossipov and J. Hilborn, *Carbohydr. Polym.*, 2018, **197**, 641–648.
59 M. H. Bakker, C. C. S. Tseng, H. M. Keizer, P. R. Seevinck, H. M. Janssen, F. J. Van Slochteren, S. A. Chamuleau and P. Y. W. Dankers, *Adv. Healthcare Mater.*, 2018, **7**, 1701139.
60 M. Fragai, E. Ravera, F. Tedoldi, C. Luchinat and G. Parigi, *ChemPhysChem*, 2019, **20**, 2204–2209.
61 A. Dasgupta and D. Das, *Langmuir*, 2019, **35**, 10704–10724.
62 M. J. Webber, J. A. Kessler and S. I. Stupp, *J. Intern. Med.*, 2010, **267**, 71–88.
63 A. Altunbas and D. J. Pochan, *Top. Curr. Chem.*, 2012, **310**, 135–167.
64 A. Accardo, D. Tesauro and G. Morelli, *Polym. J.*, 2013, **45**, 481–493.
65 S. R. Bull, M. O. Guler, R. E. Bras, T. J. Meade and S. I. Stupp, *Nano Lett.*, 2005, **5**, 1–4.
66 S. R. Bull, M. O. Guler, R. E. Bras, P. N. Venkatasubramanian, S. I. Stupp and T. J. Meade, *Bioconjugate Chem.*, 2005, **16**, 1343–1348.
67 A. T. Preslar, G. Parigi, M. T. McClendon, S. S. Sefick, T. Y. Moyer, C. R. Haney, E. A. Waters, K. W. MacRenaris, C. Luchinat, S. I. Stupp and T. J. Meade, *ACS Nano*, 2014, **8**, 7325–7332.
68 D. Qureshi, S. K. Nayak, S. Maji, A. Anis, D. Kim and K. Pal, *Eur. Polym. J.*, 2019, **120**, 109220.
69 Z. Liu, C. Wang, G. Wu and J. Cheng, *Biochem. Biophys. Res. Commun.*, 2019, **509**, 529–534.
70 K. Liu, S. Zang, R. Xue, J. Yang, L. Wang, J. Huang and Y. Yan, *ACS Appl. Mater. Interfaces*, 2018, **10**, 4530–4539.
71 A. T. Speidel, D. J. Stuckey, L. W. Chow, L. H. Jackson, M. Noseda, M. Abreu Paiva, M. D. Schneider and M. M. Stevens, *ACS Cent. Sci.*, 2017, **3**, 338–348.
72 Y. Hua, G. Pu, C. Ou, X. Zhang, L. Wang, J. Sun, Z. Yang and M. Chen, *Sci. Rep.*, 2017, **7**, 40172.
73 E. Gallo, C. Diaferia, E. D. Gregorio, G. Morelli, E. Gianolio and A. Accardo, *Pharmaceuticals*, 2020, **13**, 19.
74 P. Marckmann, L. Skov, K. Rossen, A. Dupont, M. B. Damholt, J. G. Heaf and H. S. Thomsen, *J. Am. Soc. Nephrol.*, 2006, **17**, 2359–2362.
75 E. Gianolio, P. Bardini, F. Arena, R. Stefania, E. Di Gregorio, R. Iani and S. Aime, *Radiology*, 2017, **285**, 839–849.
76 I. Pashkunova-Martic, C. Kremser, M. Galanski, V. Arion, P. Debbage, W. Jaschke and B. Keppler, *Mol. Imaging Biol.*, 2011, **13**, 16–24.
77 T. Courant, V. G. Roullin, C. Cadiou, M. Callewaert, M. C. Andry, C. Portefaix, C. Hoeffel, M. C. de Goltstein, M. Port, S. Laurent, L. V. Elst, R. Muller, M. Molinari and F. Chuburu, *Angew. Chem., Int. Ed. Engl.*, 2012, **51**, 9119–9122.
78 M. Callewaert, V. G. Roullin, C. Cadiou, E. Millart, L. Van Gulik, M. C. Andry, C. Portefaix, C. Hoeffel, S. Laurent, L. V. Elst, R. Muller, M. Molinari and F. Chuburu, *J. Mater. Chem. B*, 2014, **2**, 6397–6405.
79 G. Rigaux, C. V. Gheran, M. Callewaert, C. Cadiou, S. N. Voicu, A. Dinischiotu, M. C. Andry, L. V. Elst, S. Laurent, R. N. Muller, A. Berquand, M. Molinari, S. Huclier-Markai and F. Chuburu, *Nanotechnology*, 2017, **28**, 055705.
80 C. V. Gheran, G. Rigaux, M. Callewaert, A. Berquand, M. Molinari, F. Chuburu, S. N. Voicu and A. Dinischiotu, *Nanomaterials*, 2018, **8**, 201.
81 T. Jahanbin, H. Sauriat-Dorizon, P. Spearman, S. Benderbous and H. Korri-Youssoufi, *Mater. Sci. Eng., C*, 2015, **52**, 325–332.
82 V. V. Boroujeni, H. Hejazinia, S. E. S. Ebrahimi, M. P. Hamedani and M. S. Ardestani, *J. Pharm. Res.*, 2018, **7**, 153–159.
83 M. Russo, P. Bevilacqua, P. A. Netti and E. Torino, *Sci. Rep.*, 2016, **6**, 37906.
84 M. Russo, P. Bevilacqua, P. A. Netti and E. Torino, *Mol. Imaging*, 2017, **16**, 1–3.
85 D. Vecchione, A. M. Grimaldi, E. Forte, P. Bevilacqua, P. A. Netti and E. Torino, *Sci. Rep.*, 2017, **7**, 45121.

86 A. J. Shuhendler, R. Staruch, W. Oakden, C. R. Gordijo, A. M. Rauth, G. J. Stanisz, R. Chopra and X. Y. Wu, *J. Controlled Release*, 2012, **157**, 478–484.
87 G. Wu, H. Zhang, Z. Zhan, Q. R. Lu, J. Cheng, J. Xu and J. Zhu, *Chin. J. Chem.*, 2015, **33**, 1153–1158.
88 J. Lux, M. Chan, L. V. Elst, E. Schopf, E. Mahmoud, S. Laurent and A. Almutairi, *J. Mater. Chem. B*, 2013, **1**, 6359–6364.
89 M. Chan, J. Lux, T. Nishimura, K. Akiyoshi and A. Almutairi, *Biomacromolecules*, 2015, **16**, 2964–2971.
90 A. Soleimani, F. Martinez, V. Economopoulos, P. J. Foster, T. J. Scholl and E. R. Gillies, *J. Mater. Chem. B*, 2013, **1**, 1027–1034.
91 W. Sun, S. Thies, J. Zhang, C. Peng, G. Tang, M. Shen, A. Pich and X. Shi, *ACS Appl. Mater. Interfaces*, 2017, **9**, 3411–3418.
92 H. Wang, T. T. Dai, B. L. Lu, S. L. Li, Q. Lu, V. Mukwaya and H. J. Dou, *Chin. J. Polym. Sci.*, 2018, **36**, 391–398.
93 C. K. Lim, A. Singh, J. Heo, D. Kim, K. E. Lee, H. Jeon, J. Koh, I. C. Kwon and S. Kim, *Biomaterials*, 2013, **34**, 6846–6852.
94 K. Podgórna, K. Szczepanowicz, M. Piotrowski, M. Gajdošová, F. Štěpánek and P. Warszyński, *Colloids Surf., B*, 2017, **153**, 183–189.
95 C. Caro, M. L. García-Martín and M. P. Leal, *Biomacromolecules*, 2017, **18**, 1617–1623.
96 X. Zhao, L. Zeng, N. Hosmane, Y. Gong and A. Wu, *Chin. Chem. Lett.*, 2019, **30**, 87–89.
97 Y. Zhang, H. Huang, H. Fu, M. Zhao, Z. Wu, Y. Dong, H. Li, Y. Duan and Y. Sun, *RSC Adv.*, 2019, **9**, 33302–33309.
98 J. Qin, G. Liang, B. Feng, G. Wang, N. Wu, Y. Deng, A. A. Elzatahry, A. Alghamdi, Y. Zhao and J. Wei, *Chin. Chem. Lett.*, 2020, DOI: 10.1016/j.cclet.2020.05.021.